2014 11th IEEE International
Conference on Control & Automation (ICCA)
June 18-20, 2014. Taichung, Taiwan

Biomimetic Joint/Task Space Hybrid Adaptive Control for Bimanual Robotic Manipulation

Alex Smith, Chenguang Yang, Hongbin Ma, Phil Culverhouse, Angelo Cangelosi, Etienne Burdet

***Abstract*—In this paper, we study the adaptive control of a bimanual manipulator moving a dynamic object through a trajectory. Impedance and force are adapted online using a novel biomimetic algorithm that minimises both tracking error and control effort, as observed in humans. On top of our previous work of impedance and force adaptation, a new task space/joint-space hybrid control scheme is developed. The task space controller adapts end-point impedance, to compensate for interactive dynamics, and the joint-space controller adapts the impedance to improve robustness against external disturbances. Extensive simulations demonstrate the efficiency of the developed adaptive motion controller. The results show that the proposed hybrid controller can perform well under large disturbance conditions while minimising control effort and tracking error.**

I. Introduction

In the past most research within robot control has been focused on accurate, repeatable and stiff movement; this can be attributed to most robots being used within industry, moving in free space to improve quality assurance and reduce manufacturing costs [1]. Tasks such as welding, spray painting and pick-and-place operations generally do not place any uncertain dynamics upon the robot, as well as having a set path or several set paths to work along. This allows for simple control methods, i.e. PID control [2] to reach joint positions, and removes the need for computationally expensive inverse kinematics.

However, as the application field has been expanded, modern robots will interact with fragile objects, other machines and even humans [3] [4]. In addition, manipulators can be highly redundant [5] or under-actuated [6], creating new avenues of robot control problems. Interaction with the environment, such as objects or humans, requires feedback to allow the robot to maintain its objective while compensating for disturbance from obstacles [7]. Furthermore, the future proliferation of robots within our natural environment requires manipulator design to follow that of a human, i.e. it is easier to change the robot, than to change our entire environment. Hence, a robot with two arms gives the ability to perform a much wider range of tasks than if it only had the use of one arm, such as lifting heavy objects or carrying delicate items. In addition, with certain tool tasks, such as drilling or carving, the force required to perform the action can be spread across two manipulators, reducing the complexity and cost of the manipulator design.

A. Smith, C. Yang, P. Culverhouse, and A. Cangelosi are with School of Computing and Mathematics, Plymouth University , UK, PL4 8AA, E-mail: cyang@ieee.org; C. Yang and H. Ma are with School of Automation, Beijing Institute of Technology, Beijing, China, 100081, E-mail: mathmhb@bit.edu.cn; E. Burdet is with Department of Bioengineering, Imperial College London, SW7 2AZ, UK, E-mail: e.burdet@imperial.ac.uk.

This work is supported in part by EU grant PIIFR-GA-2010-910078; Royal Society research grant RG130244; EPSRC BABEL project and the EU grant FP7-ICT-601003 BALANCE. This work is also partially supported by NSFC under Grants 61004059, Beijing Outstanding Talents Programme (2012D009011000003) as well as China-UK NSFC-RS Joint Project under Grants 61211130359 (China) and IE111175 (UK).

TABLE I
Nomenclature

Symbol	Description
q_L, q_R	joint angle: left and right arm
$\dot{q}_L, \dot{q}_R$	joint velocity: left and right arm
X_L, X_R	Cartesian position: left and right arm
$\dot{X}_L, \dot{X}_R$	Cartesian velocity: left and right arm
l	natural ball spring length
m, k, d	object mass, stiffness and damping, respectively
F_L, F_R	forces at left, right hand respectively
F_{int}, F_{ext}	internal, external force respectively
e, e_x	joint and task-space position error, respectively
ε	tracking error
$\|\cdot\|$	Euclidean vector norm
$0_{m\times m}$	$m \times m$-dimensional zero matrix
n	Number of manipulator joints

More recently, research into impedance control has been focused on adaptation, i.e. online adjustment of stiffness and damping of the manipulator [8]. This is largely due to research which reveals the fact that the human central nervous system (CNS) adapts impedance to achieve various tasks [9–13]. Burdet et al. [14] demonstrated that humans are able to learn to stabilise unstable dynamics using energy-efficient, selective control of impedance geometry. As a matter of fact, the CNS can change the magnitude and geometry of endpoint stiffness through selective activation of agonist and antagonist muscles, to maintain stability and minimise energy expenditure. The observation of human motor control experiments inspired our research on robot control design. A complete theoretical framework of human-like adaptation of force and impedance has been established in [8], which we extend to hybrid control of the bimanual robot in this paper.

II. Problem Formulation

A scenario is posed where two robot manipulators are placed next to each other, so that a large portion of their workspaces are shared. The task is for the two robots to work cooperatively, to move a object with unknown internal dynamics, e.g., vibration, through a trajectory. The object dynamics are modelled as a mass-spring-damper system, as shown in Fig. 1. The object exerts a high frequency, low amplitude disturbance force to the end effectors, in the same way a vibrating tool might. In addition, a second disturbance force is applied proximally; that is, an external collision force. This second force is modelled as a low frequency, high amplitude disturbance acting upon the first link of the robot. The controller is required to closely follow the trajectory, i.e. minimise tracking error, as well as minimise "metabolic" cost. This is achieved through the use of a biomimetic controller.

A. Object Dynamics

The dynamics model of the object is presented in this section. For simplicity but without loss of generality, the shape

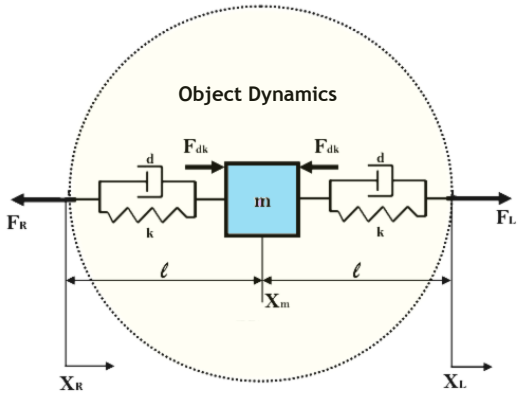

Fig. 1. Diagram of object dynamics, modeled as a mass-spring-damper system. F_R and F_L are the interaction forces acting on the left and right arms as a result of the Cartesian positions and velocities of the left and right end-effectors.

of the object is assumed to be a sphere. The interaction forces F_R and F_L resulting from the object dynamics are described with reference to the Cartesian position and velocity of the central mass, and left and right end-effectors $X, \dot{X}$ respectively.

$$\begin{aligned} F_R &= -k\big(l - (X_m - X_R)\big) - d(\dot{X}_R - \dot{X}_m) \\ F_L &= k\big(l - (X_L - X_m)\big) - d(\dot{X}_m - \dot{X}_L) \end{aligned} \tag{1}$$

That is, the forces acting at each of the left and right hand, are the sum of forces arising from interaction of the mass of the object and the hand upon the spring-damper system distributed equally across the surface of the object. From Newton's Second Law of motion, we have

$$-m\ddot{X}_m = F_L + F_R \tag{2}$$

which together with (1) yields

$$-m\ddot{X}_m = 2d\dot{X}_m + 2kX_m - d(\dot{X}_L + \dot{X}_R) - k(X_L + X_R) \tag{3}$$

For convenience, the object dynamics are formed into a state space representation with X_m and $\dot{X}_m$ as the states, and X_L, X_R, $\dot{X}_L$ and $\dot{X}_R$ as the inputs:

$$\begin{bmatrix} \dot{X}_m \\ \ddot{X}_m \end{bmatrix} = \begin{bmatrix} 0 & 1 \\ \frac{-2k}{m} & \frac{-2d}{m} \end{bmatrix} \begin{bmatrix} X_m \\ \dot{X}_m \end{bmatrix} + \begin{bmatrix} 0 & 0 & 0 & 0 \\ \frac{k}{m} & \frac{k}{m} & \frac{d}{m} & \frac{d}{m} \end{bmatrix} \begin{bmatrix} X_L \\ X_R \\ \dot{X}_L \\ \dot{X}_R \end{bmatrix} \tag{4}$$

The formulation of the outputs F_L and F_R is given by:

$$\begin{bmatrix} F_L \\ F_R \end{bmatrix} = \begin{bmatrix} k & d \\ k & d \end{bmatrix} \begin{bmatrix} X_m \\ \dot{X}_m \end{bmatrix} + \begin{bmatrix} -k & 0 & -d & 0 \\ 0 & -k & 0 & -d \end{bmatrix} \begin{bmatrix} X_L \\ X_R \\ \dot{X}_L \\ \dot{X}_R \end{bmatrix} + \begin{bmatrix} kl \\ -kl \end{bmatrix} \tag{5}$$

The dynamics of the object shown in (4) and (5) can be changed by specifying the mass, stiffness and damping m, k, d respectively.

B. Robot Dynamics

The robot dynamics of left and right arms are given as:

$$\begin{aligned} M_L(q_L)\ddot{q}_L + C_L(q_L, \dot{q}_L)\dot{q}_L + G_L(q_L) &= \tau_{u_L} + f_L \\ M_R(q_R)\ddot{q}_R + C_R(q_R, \dot{q}_R)\dot{q}_R + G_R(q_R) &= \tau_{u_R} + f_R \end{aligned} \tag{6}$$

where $q_{L,R}$ denote the joint position of left and right robot arm, respectively; $M_{L,R}(q) \in \mathbb{R}^{n\times n}$ is the symmetric bounded positive definite inertia matrix, and n is the degree of freedom (DoF) of the robot arm; $C_{L,R}(q, \dot{q})\dot{q} \in \mathbb{R}^n$ denotes the Coriolis and Centrifugal force; $G_{L,R}(q) \in \mathbb{R}^n$ is the gravitational force; $\tau_{u_{L,R}} \in \mathbb{R}^n$ is the vector of control input torque; and $f_{L,R} \in \mathbb{R}^n$ is the external force caused by friction, disturbance or load etc. The control torque $\tau_{u_{L,R}}$ is generated by the controller to be designed, in order to achieve desired performance in terms of motion tracking and disturbance rejection.

III. Bimanual Control with Adaptive Impedance and Force

A. Trajectory Generation

A smooth trajectory [15] is defined in Cartesian space as

$$\begin{aligned} y^*(t) &= y^*(0) + \big(y^*(T) - y^*(0)\big)G \\ G &= 10\left(\frac{2t}{T}\right)^3 - 15\left(\frac{2t}{T}\right)^4 + 6\left(\frac{2t}{T}\right)^5 \end{aligned} \tag{7}$$

where $y^*(0)$ is the start point of the curve, $y^*(T)$ is the final point, and T is the period of the trajectory. The desired Cartesian trajectory of the left (leading) arm is represented by a vector $X_L^* \in \mathbb{R}^{6\times 1}$:

$$X_L^* = [x_L^*\ y_L^*\ z_L^*\ \vartheta_L^*\ \phi_L^*\ \psi_L^*]^T \tag{8}$$

The initial position of the end-effector of the left arm, $X_L(0) = fkine\big(q_L(0)\big)$, with $fkine(\cdot)$ denoting the forward dynamics, defines the x_L, z_L, ϑ_L, ϕ_L and ψ_L components of (8) so that the arm moves in the y-plane along the trajectory defined from (7):

$$X_L^*(t) = \Big[x_L(0)\ y_L^*(t)\ z_L(0)\ \vartheta_L(0)\ \phi_L(0)\ \psi_L(0)\Big]^T \tag{9}$$

The Cartesian velocity, required for inverse kinematics in (11), is the first differential of $X_L^*(t)$ defined in (9):

$$\dot{X}_L^*(t) = \frac{\mathrm{d}}{\mathrm{d}t} X_L^*(t) \tag{10}$$

Joint space angular velocity $\dot{q}_L^*$ is defined through the inverse Jacobian and the first differential of the Cartesian trajectory:

$$\dot{q}_L^* = J^{-1}(q_L)\dot{X}_L^* \tag{11}$$

Joint angles and accelerations are the integration and differentiation of joint velocity, respectively:

$$\begin{aligned} q_L^* &= \int \dot{q}_L^*\, \mathrm{d}t \\ \ddot{q}_L^* &= \frac{\mathrm{d}}{\mathrm{d}t}\, \dot{q}_L^* \end{aligned} \tag{12}$$

The desired trajectory of the right (following) hand, X_R^* is defined as an offset in the y-plane from the left hand:

$$X_R^* = \Big[x_L(t)\ \big(y_L(t) + p^*\big)\ z_L(t)\ \vartheta_L(t)\ \phi_L(t)\ \psi_L(t)\Big]^T \tag{13}$$

where p^* is the desired distance between the end-effectors of left and right manipulators. Following the same calculation as above, we obtain q_L^*, $\dot{q}_L^*$ and $\ddot{q}_L^*$.

B. Adaptive Control Law

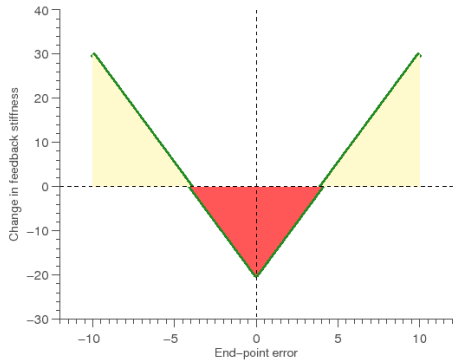

Fig. 2. Change in endpoint stiffness, i.e. δK follows a "V-shaped" adaptation [16]. The lighter shaded areas indicate where the error is above an error threshold, so stiffness increases; the darker shaded area indicates where the error is acceptable, so stiffness is reduced, which in turn reduces applied effort.

The adaptive law has been designed to minimise motion tracking error, whilst also minimising control effort. The adaptation of stiffness and damping follows the work by Franklin et al. [16], which shows that human motor control is based on simultaneous optimisation of stability, accuracy and efficiency; the "V-shaped" learning function can be seen in Fig. 2. Here this adaptation is continuous so that error and effort are continuously minimised. The controller developed in [8] has been adapted in this paper to be applied to dual arm manipulation, as an extension of the previous single robot arm application. It should be noted that the controllers defined below will be applied to both left and right manipulators, and thus the subscripts "L" and "R" are omitted for convenicence.

1) Feedfoward Compensation and Minimum Feedback : Given the dynamics of a manipulator in (6), we employ the following controller as a basic torque input

$$\tau_r(t) = M(q)\ddot{q}^* + C(q,\dot{q})\dot{q}^* + G(q) - L(t)\varepsilon(t) \tag{14}$$

where $L(t)\varepsilon(t)$ corresponds to the desired *stability margin*, and the first three terms are feedforward compensation. As widely used in sliding mode control, we define tracking error $\varepsilon(t)$ as below

$$\varepsilon(t) = \dot{e}(t) + \kappa e(t)$$

where $e(t)$ and $\dot{e}(t)$ are joint errors to be defined in (16). On top of the above control input $\tau_r(t)$, we develop two adaptive controllers in joint space and task space, respectively.

2) Joint Space Adaptive Control: We apply joint space controller from [8] as below:

$$\tau_j(t) = -\tau(t) - K(t)e(t) - D(t)\dot{e}(t) \tag{15}$$

with

$$e(t) = q(t) - q^*(t),\ \dot{e}(t) = \dot{q}(t) - \dot{q}^*(t) \tag{16}$$

where $-\tau(t)$ is the learned *feedforward* torque, $-K(t)e(t)$ and $-D(t)\dot{e}(t)$ are *feedback* torques due to stiffness and damping respectively. We apply the adaptive law developed in [8] (but here in the time domain, rather than iteration, making the controller applicable to non-periodic tasks) as follows:

$$\begin{aligned}
\delta\tau(t) &= \tau(t) - \tau(t-\delta t) = Q_\tau\varepsilon(t) - \gamma\tau(t)\\
\delta K(t) &= K(t) - K(t-\delta t) = Q_K\varepsilon(t)e^T(t) - \gamma K(t)\\
\delta D(t) &= D(t) - D(t-\delta t) = Q_D\varepsilon(t)\dot{e}^T(t) - \gamma D(t)
\end{aligned} \tag{17}$$

where γ is defined as the forgetting factor

$$\gamma = \frac{a}{1 + b\|\varepsilon(t)\|^2} \tag{18}$$

Given that $K(0) = 0_{[n,n]}$ and $D(0) = 0_{[n,n]}$, and Q_K, Q_D are diagonal positive-definite constant gain matrices.

3) Task Space Adaptive Control: From (9) and (13) we can see that the movement of the object is described by a Cartesian trajectory, so it is more useful to describe the control in terms of Cartesian rather than joint errors. This makes control of impedance in Cartesian space much more straightforward. First, we redefine our error terms to be in Cartesian, rather than joint space

$$\begin{aligned}
e_x(t) &= X(t) - X^*(t)\\
\dot{e}_x(t) &= \dot{X}(t) - \dot{X}^*(t)\\
\varepsilon_x(t) &= \dot{e}_x(t) + \kappa e_x(t)
\end{aligned} \tag{19}$$

This leads to a change in the *feedforward* and *feedback* terms described in (17) with γ_x defined similarly as in (18)

$$\begin{aligned}
\delta F_x &= Q_F\,\varepsilon_x - \gamma_x F_x\\
\delta K_x &= Q_{K_x}\,\varepsilon_x e_x - \gamma_x K_x\\
\delta D_x &= Q_{D_x}\,\varepsilon_x \dot{e}_x - \gamma_x D_x
\end{aligned} \tag{20}$$

These terms can be described as a sum of forces F_{xkd} where

$$F_{xkd} = -F_x - K_x e_x - D_x \dot{e}_x \tag{21}$$

which can be transformed into joint space using the equation below:

$$\tau_x = J^T(q)\,F_{xkd} \tag{22}$$

where $J(q)$ is the Jacobian satisfying $\dot{x} \equiv J(q)\dot{q}$.

Combination of the basic controller (14), the joint space controller (15) and the task space controller (22) gives us

$$\tau_u(t) = \tau_j(t) + \tau_x(t) + \tau_r(t) \tag{23}$$

IV. Adaptive Control with Internal Interaction

In this section, we focus on the case that only an internal interaction force is applied, that is, the two arms are subjected to forces at the end-effector, arising from the dynamic properties of the object modeled in (4) and (5), as well as a high frequency, low amplitude perturbation F_{int}. This perturbation force is defined as a sine wave acting in the plane of movement, described in (9)

$$\begin{aligned}
F_{int} &= [0 \quad y_{int} \quad 0 \quad 0 \quad 0 \quad 0]^T\\
y_{int} &= A_{int}\sin(2\pi f_{int} t)
\end{aligned} \tag{24}$$

where $0 < A_{int} \leq 10$ is the amplitude and $100 < f_{int} \leq 1000$ is the frequency of oscillation in Hertz. The forces applied to each arm F_{int_L}, F_{int_R} are only the negative and positive components, respectively

$$\begin{aligned}
F_{int_L} &= \begin{cases} y_{int} & \text{if } y_{int} < 0 \\ 0 & \text{if } y_{int} \geq 0 \end{cases}\\
F_{int_R} &= \begin{cases} 0 & \text{if } y_{int} \leq 0 \\ y_{int} & \text{if } y_{int} > 0 \end{cases}
\end{aligned} \tag{25}$$

Effectively, this simulates the object bouncing between the hands, only *pushing against* the hands, not *pulling*, as shown in Fig. 6. To compensate for the effect of internal interaction, we only consider task space adaptive control together with basic control, i.e.,

$$\tau_u(t) = \tau_x(t) + \tau_r(t) \tag{26}$$

A. Simulation and Results

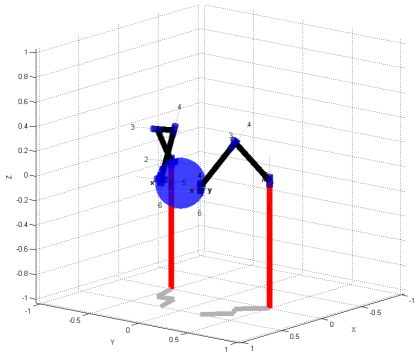

Fig. 3. MATLAB figure showing the modeled twin *Puma 560* manipulators holding the object, in blue.

Simulations are carried out using the MATLAB Robotics Toolbox developed in [17] with twin Puma 560 models, which can be seen in Fig. 3. In this paper, we focus on the manipulation control along the task trajectory, and thus the effect of gravity acting on the object can be ignored (as if the object is moving on top of a table), but the object can be assumed to be dropped if the distance between the end-effectors of the manipulators becomes larger than the diameter of the object. The controller parameters are selected as

$$\begin{aligned} Q_F &= diag\big([10\ 10\ 10\ 1\ 1\ 1]\big) \\ Q_{K_x} &= diag\big([5\ 20\ 1\ 10\ 0.1\ 0.1]\big) \times 10^3 \\ Q_{D_x} &= diag\big([1\ 1\ 1\ 1\ 1\ 5]\big) \\ a &= 0.2, \quad b = 3, \quad \kappa = 20 \end{aligned} \tag{27}$$

and

$$L = diag\big([5\ 10\ 20\ 1\ 1\ 1]\big) \tag{28}$$

The parameters for the trajectory defined in (7), $y^*(0) = y_L(0)$, $y^*(T) = y_L(0) - 0.2m$, $T = 4.8sec$. The radius of the object is set at $r = 0.25m$, with the initial positions of the arms $X_L(0)$ and $X_R(0)$ set so the Euclidean distance between the hands, that is, $h = \|X_L(0) - X_R(0)\|$ is slightly smaller than the diameter of the object. This value also sets the desired distance between the hands throughout the trajectory, p^*, as shown in (13). The value h can therefore be used to determine if the object is in the grasp; if $h \geq 2r$ then the object is dropped. In addition, if the controller becomes unstable, the simulation is stopped. In Fig. 4 we compare a controller with no adaptation to our adaptive method. As can be seen from the time scales, without adaptive feedback the controller is unable to complete the task, and tracking errors increase very rapidly. In contrast, the proposed adaptive controller is able to complete the task with very small tracking error from the desired trajectory. Fig. 5 shows the adapted parts of the controller. It can be noted that the green trace in Fig. 5 is the y-axis, so a larger increase in gain is expected due to the majority of disturbance forces being encountered in this plane. Also, it can be seen that these values will tend towards zero when there is little error, minimising effort and maintaining stability.

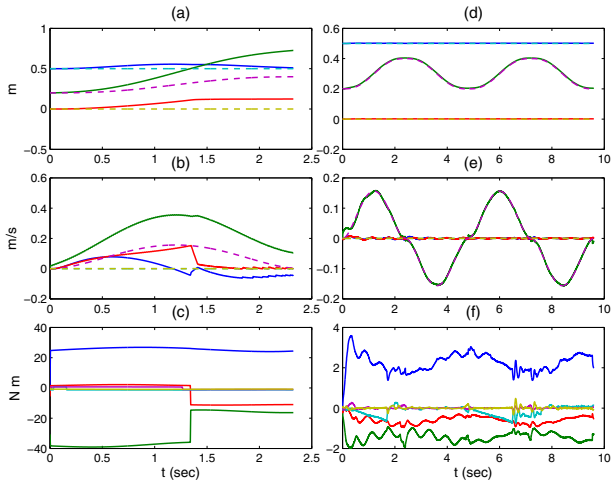

Fig. 4. $A_{int} = 10$N, $f_{int} = 50$Hz. Solid lines in (a), (b), (d) and (e) are actual values while dashed lines are desired. Graphs (a), (b) and (c) show the Cartesian position, velocity and input torque to the arm **without** adaptation; (d), (e) and (f) show the corresponding values with adaptation.

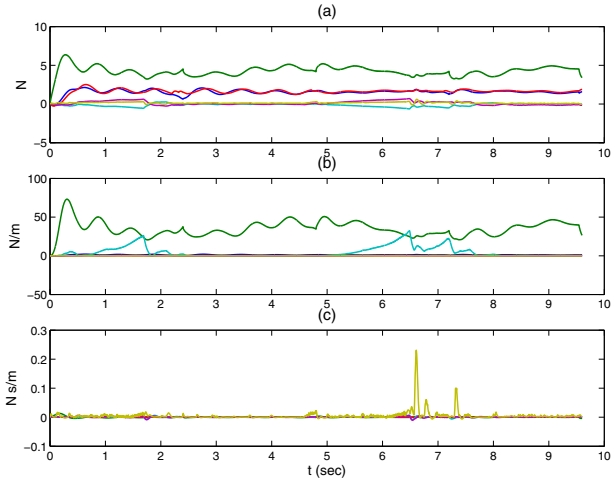

Fig. 5. Adapted feedforward force F_x (a) and the diagonal elements of the stiffness matrix K_x (b), and damping matrix D_x (c) for the left arm; the x, y, z components in blue, green, red, respectively, $roll, pitch, yaw$ components in cyan, purple and orange, respectively.

V. Adaptive Control with Both Internal and External Interaction

Further to the previous simulation study, a second disturbance force F_{ext} is applied, as discussed in Section II and can be seen in Fig. 6, where

$$\begin{aligned} F_{ext} &= [x_{ext} \quad y_{ext} \quad z_{ext} \quad 0 \quad 0 \quad 0]^T \\ x_{ext} &= y_{ext} = z_{ext} = A_{ext} \sin(2\pi f_{ext} t) \end{aligned} \tag{29}$$

where $10 < A_{ext} \leq 100$ is the amplitude of perturbation and $0.1 < f_{ext} \leq 10$ is the frequency. To simulate this force being applied at the "elbow", the following equation is used

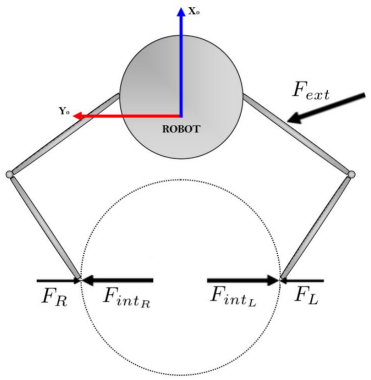

Fig. 6. Diagram of interaction forces acting on the manipulator pair. F_L and F_R are the *passive* forces caused by dynamic interaction with the object. F_{int_L} and F_{int_R} are the high frequency, low amplitude forces caused by *active* vibration of the object. F_{ext} is the external force modelling contact with the environment.

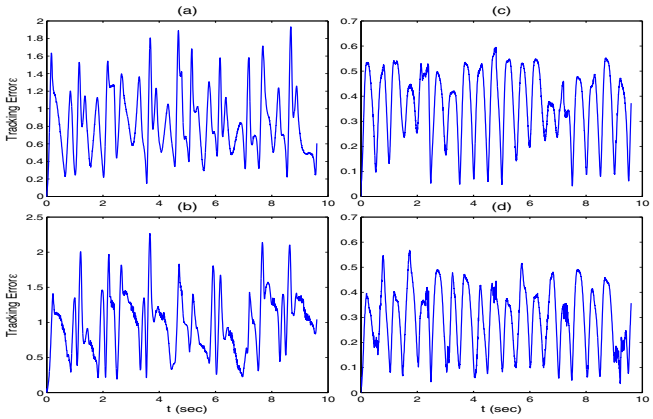

Fig. 7. Graphs (a), (b) show the 2-norm of the tracking error, $||\varepsilon_x||$, from the purely task space controller, for the left and right end-effectors respectively. Graphs (c), (d) show the respective tracking error norm when simulated with the hybrid controller.

to calculate the torque caused by the external force F_{ext}

$$\tau_{ext} = \Gamma\, J^T(q) F_{ext} \tag{30}$$

where the reduction matrix Γ is defined as

$$\Gamma = diag\big([1\,1\,0\,0\,0\,0\,]\big) \tag{31}$$

To improve robustness against this second disturbance force, now we bring in the joint space adaptive controller to work concurrently with the task space controller, as we are concerned about the joint positions of the shoulder joints rather than their positions in task space. The feedforward and feedback terms in (17) are applied, but with the gains pre-multiplied so that the controller only acts on the first two joints above "elbow" as below:

$$\begin{aligned}
\delta\tau_{sh}(t) &= \Gamma\,\big(Q_\tau\,\varepsilon(t) - \gamma(t)\tau_{sh}(t)\big)\\
\delta K_{sh}(t) &= \Gamma\,\big(Q_K\,\varepsilon(t)e^T(t) - \gamma(t)K_{sh}(t)\big)\\
\delta D_{sh}(t) &= \Gamma\,\big(Q_D\,\varepsilon(t)\dot{e}^T(t) - \gamma(t)D_{sh}(t)\big)
\end{aligned} \tag{32}$$

These terms can now be to define a control torque in joint space for the proximal joints, τ_{prox}

$$\tau_{prox} = -\tau_{sh} - K_{sh}e - D_{sh}\dot{e} \tag{33}$$

The overall controller now becomes

$$\tau_u(t) = \tau_x(t) + \tau_{prox}(t) + \tau_r(t) \tag{34}$$

A. Simulation and Results

Gain and trajectory parameters are the same as in Section IV-A with the addition of the joint-space control gains, which are defined as

$$Q_\tau = Q_F,\; Q_K = Q_{K_x},\; Q_D = Q_{D_x} \tag{35}$$

with $f_{ext} = 1$Hz and $A_{ext} = 50$, applied equally to both arms. The internal forces F_{int_L} and F_{int_R} are the same as the previous simulation in Section IV-A. Tracking error results are compared in Fig. 7 for the task space controller and hybrid controller; it can be seen that the tracking performance is improved using the hybrid control scheme. Task-space feedforward force F_x, stiffness K_x and damping D_x are shown in Fig. 8. It can be seen that in every case these values are much reduced in the hybrid controller; in particular the stiffness and damping, which are reduced by more than ten times. The adaptive terms which form τ_j are shown in Fig.

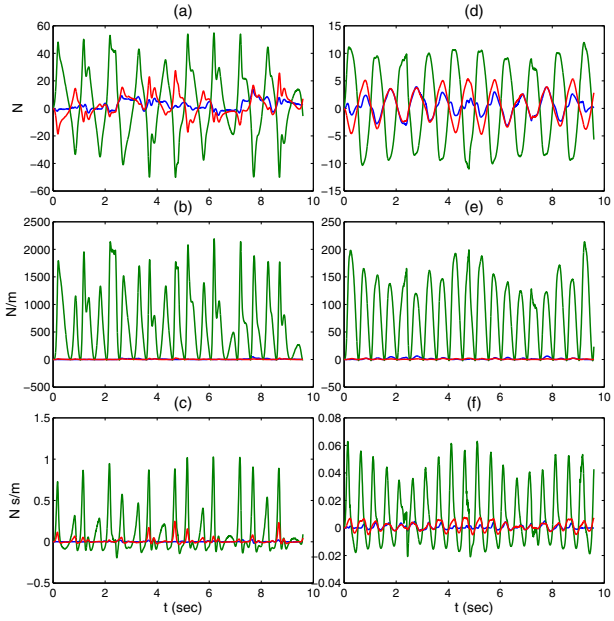

Fig. 8. Graphs (a)-(c) show F_x and diagonal components of the K_x and D_x matrices for the purely task space controller, (d)-(f) the respective adaptations for the hybrid controller, both taken from the left arm. The blue, green and red lines denote the x, y, z planes respectively.

9. Blue traces show adaptations on the first joint, which must compensate the most against the external force F_{ext}, while the green trace is the adaptation on the second shoulder joint. It can be noted that although these extra torques are applied to the arms, the sum of effort in the hybrid controller from Figs. 8 and 9 is less than that of the task space controller.

VI. Discussion and Conclusion

Two simulation studies have been carried out to test the effectiveness of the biomimetic, bimanual adaptive controller,

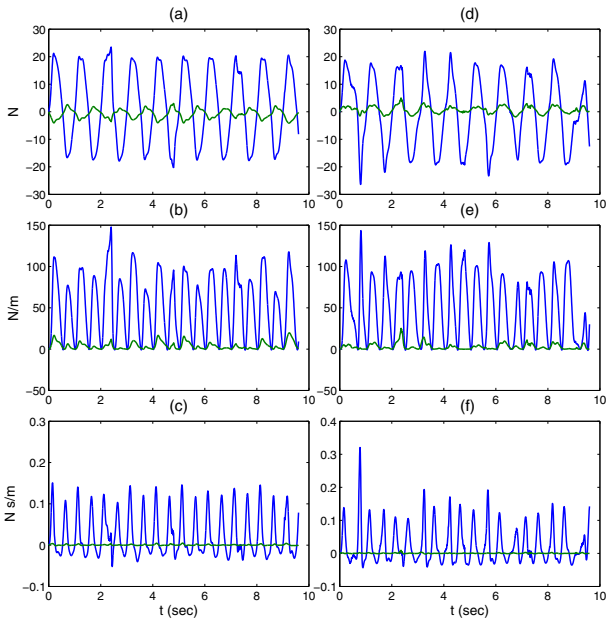

Fig. 9. Adaptive terms forming τ_j: (a) shows the progression of nonzero components of τ_{sh}, (b) the adaptation of nonzero diagonal components of K_{sh} and (c) the nonzero diagonal components of damping D_{sh} for the left arm. Graphs (d) to (f) show the same values for the right arm. The blue line is related to the first joint, and the green line the second joint.

in a task to move a vibrating object through a trajectory while under the influence of

- dynamics of the object and internal disturbance forces caused by vibration;
- dynamics of the object, internal disturbance forces and external perturbation forces.

The simulated experiments show that:

- The proposed controller can perform under conditions which are not possible without adaptation.
- Control effort and motion tracking error are minimised, creating inherent stability.
- The hybrid task-space/joint-space controller is robust when an external collision force is applied.
- Performance is improved when using the hybrid controller, in terms of control effort and tracking error.

In future work, it is planned to include the effects of gravity and grip friction into the model, as well as test the proposed hybrid adaptive controller on a physical robot.

REFERENCES

[1] M. Doms, T. Dunne, and M. J. Roberts, "The role of technology use in the survival and growth of manufacturing plants," *International Journal of Industrial Organization*, vol. 13, no. 4, pp. 523–542, 1995.

[2] V. Parra-Vega, S. Arimoto, Y.-H. Liu, G. Hirzinger, and P. Akella, "Dynamic sliding pid control for tracking of robot manipulators: theory and experiments," *Robotics and Automation, IEEE Transactions on*, vol. 19, no. 6, pp. 967–976, 2003.

[3] M. A. Peshkin, J. E. Colgate, W. Wannasuphoprasit, C. A. Moore, R. B. Gillespie, and P. Akella, "Cobot architecture," *Robotics and Automation, IEEE Transactions on*, vol. 17, no. 4, pp. 377–390, 2001.

[4] O. Lambercy, L. Dovat, R. Gassert, E. Burdet, C. L. Teo, and T. Milner, "A haptic knob for rehabilitation of hand function," *Neural Systems and Rehabilitation Engineering, IEEE Transactions on*, vol. 15, no. 3, pp. 356–366, 2007.

[5] J. S. Pettinato and H. E. Stephanou, "Manipulability and stability of a tentacle based robot manipulator," in *Robotics and Automation, 1989. Proceedings., 1989 IEEE International Conference on*. IEEE, 1989, pp. 458–463.

[6] G. Oriolo and Y. Nakamura, "Control of mechanical systems with second-order nonholonomic constraints: Underactuated manipulators," in *Decision and Control, 1991., Proceedings of the 30th IEEE Conference on*. IEEE, 1991, pp. 2398–2403.

[7] N. Hogan, "Impedance control: An approach to manipulation," in *American Control Conference, 1984*. IEEE, 1984, pp. 304–313.

[8] C. Yang, G. Ganesh, S. Haddadin, S. Parusel, A. Albu-Schäeffer, and E. Burdet, "Human-Like Adaptation of Force and Impedance in Stable and Unstable Interactions," *IEEE Transactions on Robotics*, vol. 27, no. 5, 2011.

[9] D. W. Franklin, R. Osu, E. Burdet, M. Kawato, and T. E. Milner, "Adaptation to stable and unstable dynamics achieved by combined impedance control and inverse dynamics model," *Journal of neurophysiology*, vol. 90, no. 5, pp. 3270–3282, 2003.

[10] K. P. Tee, D. W. Franklin, M. Kawato, T. E. Milner, and E. Burdet, "Concurrent adaptation of force and impedance in the redundant muscle system," *Biological cybernetics*, vol. 102, no. 1, pp. 31–44, 2010.

[11] D. W. Franklin, E. Burdet, K. P. Tee, R. Osu, C.-M. Chew, T. E. Milner, and M. Kawato, "Cns learns stable, accurate, and efficient movements using a simple algorithm," *The Journal of Neuroscience*, vol. 28, no. 44, pp. 11 165–11 173, 2008.

[12] K. P. Tee, E. Burdet, C.-M. Chew, and T. E. Milner, "A model of force and impedance in human arm movements," *Biological cybernetics*, vol. 90, no. 5, pp. 368–375, 2004.

[13] T. E. Milner and D. W. Franklin, "Impedance control and internal model use during the initial stage of adaptation to novel dynamics in humans," *The Journal of physiology*, vol. 567, no. 2, pp. 651–664, 2005.

[14] E. Burdet, R. Osu, D. W. Franklin, T. E. Milner, and M. Kawato, "The central nervous system stabilizes unstable dynamics by learning optimal impedance," *Nature*, vol. 414, no. 6862, pp. 446–449, 2001.

[15] U. Pattacini, F. Nori, L. Natale, G. Metta, and G. Sandini, "An experimental evaluation of a novel minimum-jerk cartesian controller for humanoid robots," in *2010 IEEE/RSJ international conference on intelligent robots and systems. Taipei, Taiwan*, 2010.

[16] D. W. Franklin, E. Burdet, K. P. Tee, R. Osu, C. M. Chew, T. E. Milner, and M. Kawato, "CNS learns stable, accurate, and efficient movements using a simple algorithm," *Journal of Neuroscience*, vol. 28, no. 44, pp. 11 165–11 173, 2008.

[17] P. I. Corke, *Robotics, Vision & Control: Fundamental Algorithms in Matlab*. Springer, 2011.